SUPPLEMENTARY INFORMATION

Structure of a Blm10 complex reveals common mechanisms for proteasome binding and gate opening

Kianoush Sadre-Bazzaz, Frank G. Whitby, Howard Robinson, Tim Formosa, Christopher P. Hill

Figure S1, related to Figure 1

A number of observations argue that the crystal structure is not unduly influenced by lattice contacts. First, the four Blm10 complexes in the asymmetric unit are closely similar to each other and to reconstructions by electron cryomicroscopy (Iwanczyk et al., 2006; Ortega et al., 2005). Second, conserved residues mediate stabilizing contacts between Blm10 segments that are distant in amino acid sequence (panel A). Third, Blm10 wraps around the end of the proteasome barrel to contact all seven proteasome α-subunits in an interface that buries more than 10,000 $Å^2$ of solvent accessible surface area (Figure 1E) and largely defines the Blm10 conformation. Fourth, a cluster of conserved residues from HR6 to HR9 and from HR30 to beyond HR32, contact each other and residues near the N-terminus of proteasome subunits α5 and α6 (panels B-D) to help define the pore conformation and define the relative orientations of the upper and lower turns of the Blm10 solenoid. Fifth, the 3.4Å crystal structure described here of the complex with Blm10 lacking the first 50 residues appears identical to the crystal structures of full-length Blm10 complexes with proteasome observed in two different crystal forms at lower (4.0Å and 4.4Å) resolution (data not shown).

(A) Blm10 (white) with selected linker segments that stabilize the structure (color). The close-up views illustrate the role of conserved residues (underlined, panel E) that make stabilizing interactions.
(B) Proteasome α5 and α6 N-terminal residues (black) are extended and make extensive contacts with Blm10, including residues that are conserved and also stabilize the relative orientation of the two tiers of the Blm10 solenoid.
(C) Stereoview showing details of α5 N-terminal residues and their contacts. Conserved residues are underlined.
(D) Same as panel D, but for α6 contacts.
(E) *S. cerevisiae* Blm10 sequence. Secondary structures (above) colored as in Figure 1. HEAT repeat helices are labeled 1A for helix A of HEAT repeat 1, etc. Residues disordered in the structure are indicated with a dashed line. Residues that approach the proteasome within 4.0 Å are marked with a square below; contact to α1 blue, α2 cyan, α3 green, α4 magenta, α5 orange, α6 red, α7 gray. Residues identical in *S. cerevisiae* Blm10 and human PA200 are underlined. Blm10 residues conserved in an alignment of 46 related sequences are shown on a yellow background. Conservation is defined according to the ESPript consensus (Gouet et al., 1999) from the automatic alignment, with a

few residues also defined as conserved because simple manual adjustment of gaps aligns residues that appear to be structurally important.

Proteasome residues have been highly conserved throughout evolution, especially on the α-subunit surface, with 82/112 (73%) of the proteasome residues that contact Blm10 being identical in *S. cerevisiae* and human. In contrast, the Blm10 sequence is much more divergent, with only 162/2143 (8%) of the residues conserved in the alignment indicated here. The conservation is somewhat higher at the proteasome interface, especially for residues that contact proteasome α5 and α6 subunits, where 17/62 (27%) of Blm10 residues contacting these subunits are conserved.

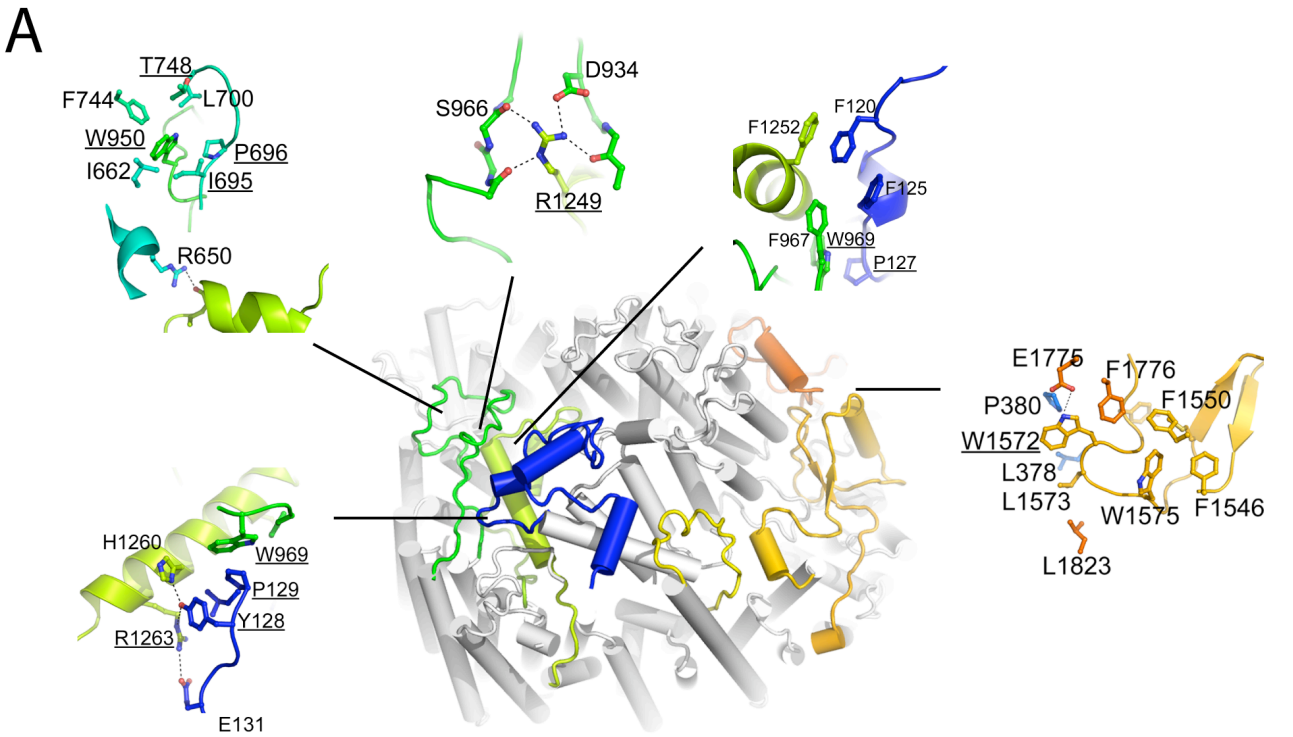
A
T748
F744
L700
W950
I662
P696
I695
R650
S966
D934
R1249
F1252
F120
F125
F967
W969
P127
E1775
F1776
P380
F1550
W1572
L378
L1573
W1575
F1546
L1823
H1260
W969
P129
Y128
R1263
E131

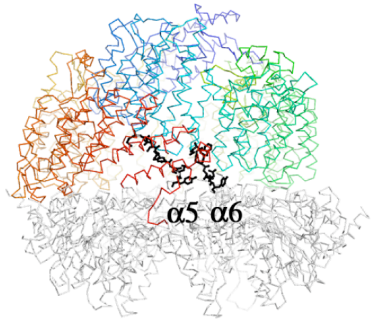
B
α5 α6

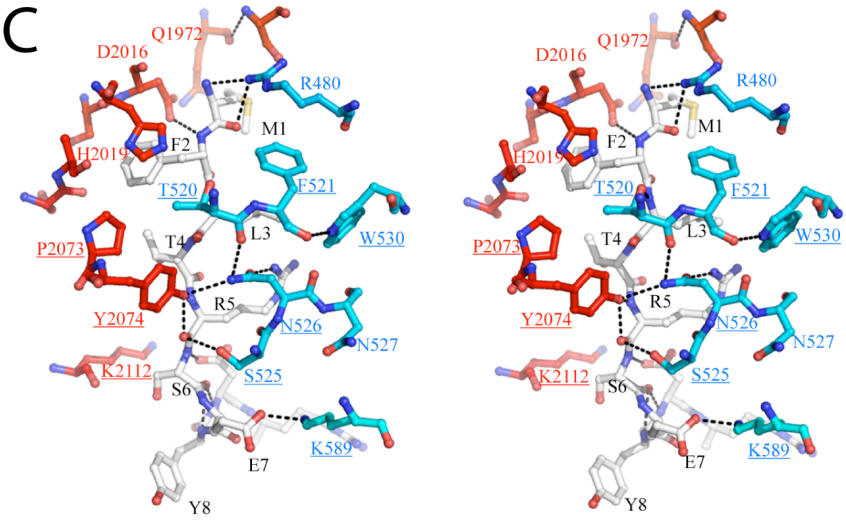
C
Q1972
D2016
R480
M1
H2019
F2
T520
F521
L3
W530
P2073
T4
R5
Y2074
N526
N527
K2112
S6
S525
K589
E7
Y8

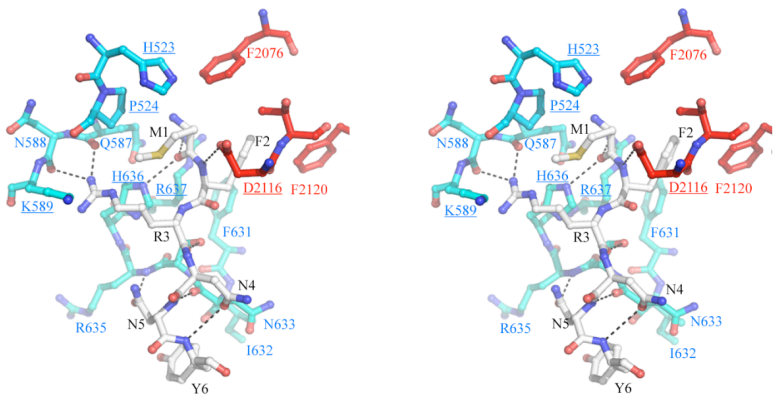
D
H523
F2076
P524
N588
Q587
M1
F2
H636
R637
D2116
F2120
K589
R3
F631
N4
R635
N5
N633
I632
Y6

E

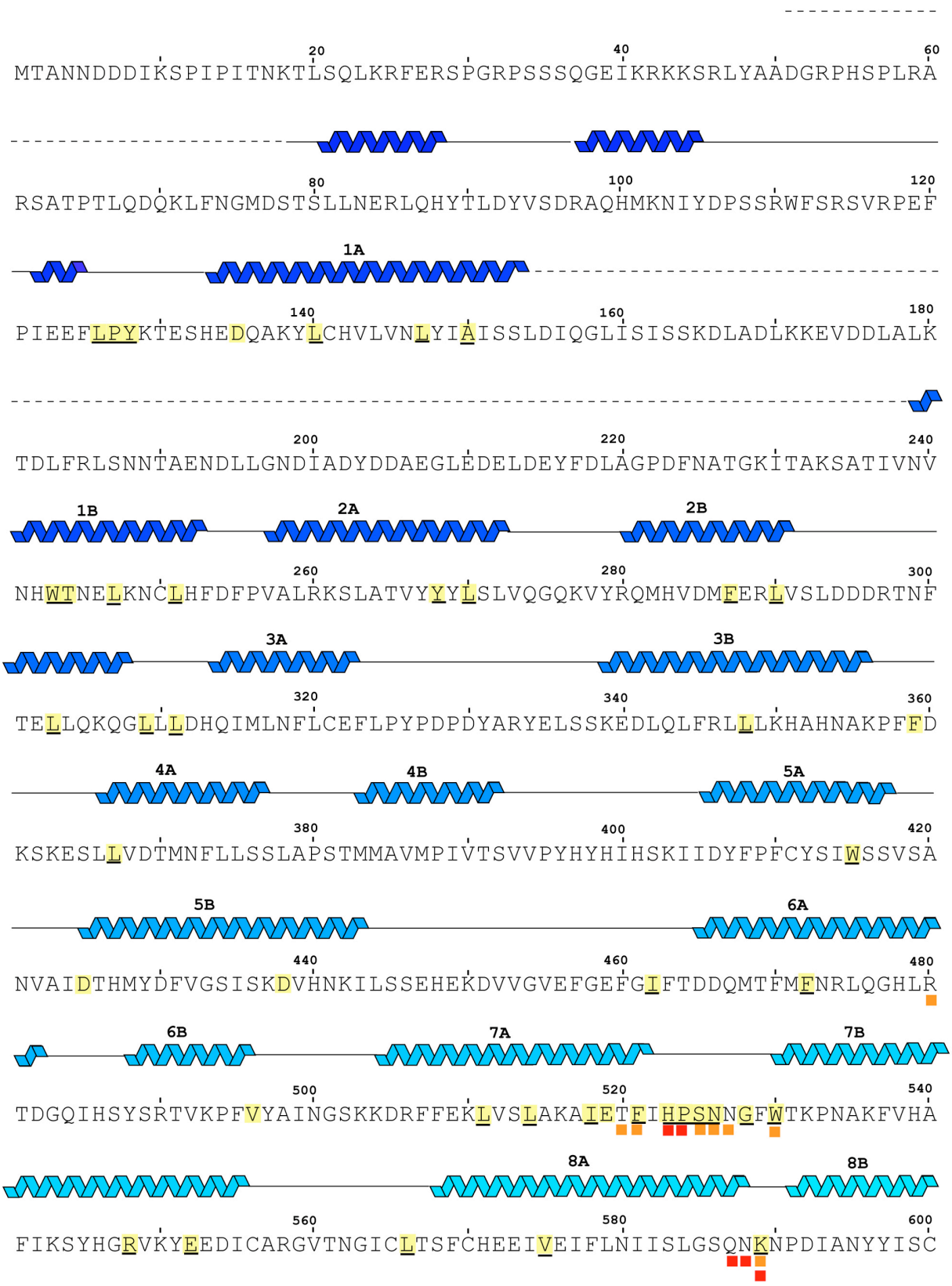
20
40
60
MTANNDDDIKSPIPITNKTLSQLKRFERSPGRPSSSQGEIKRKKSRLYAADGRPHSPLRA
80
100
120
RSATPTLQDQKLFNGMDSTSLLNERLQHYTLDYVSDRAQHMKNIYDPSSRWFSRSVRPEF
1A
140
160
180
PIEEFLPYKTESHEDQAKYLCHVLVNLYIAISSLDIQGLISISSKDLADLKKEVDDLALK
200
220
240
TDLFRLSNNTAENDLLGNDIADYDDAEGLEDELDEYFDLAGPDFNATGKITAKSATIVNV
1B
2A
2B
260
280
300
NHWTNELKNCLHFDFPVALRKSLATVYYYLSLVQGQKVYRQMHVDMFERLVSLDDDRTNF
3A
3B
320
340
360
TELLQKQGLLLDHQIMLNFLCEFLPYPDPDYARYELSSKEDLQLFRLLLKHAHNAKPFFD
4A
4B
5A
380
400
420
KSKESLLVDTMNFLLSSLAPSTMMAVMPIVTSVVPYHYHIHSKIIDYFPFCYSIWSSVSA
5B
6A
440
460
480
NVAIDTHMYDFVGSISKDVHNKILSSEHEKDVVGVEFGEFGIFTDDQMTFMFNRLQGHLR
6B
7A
7B
500
520
540
TDGQIHSYSRTVKPFVYAINGSKKDRFFEKLVSLAKAIETFIHPSNNGFWTKPNAKFVHA
8A
8B
560
580
600
FIKSYHGRVKYEEDICARGVTNGICLTSFCHEEIVEIFLNIISLGSQNKNPDIANYYISC

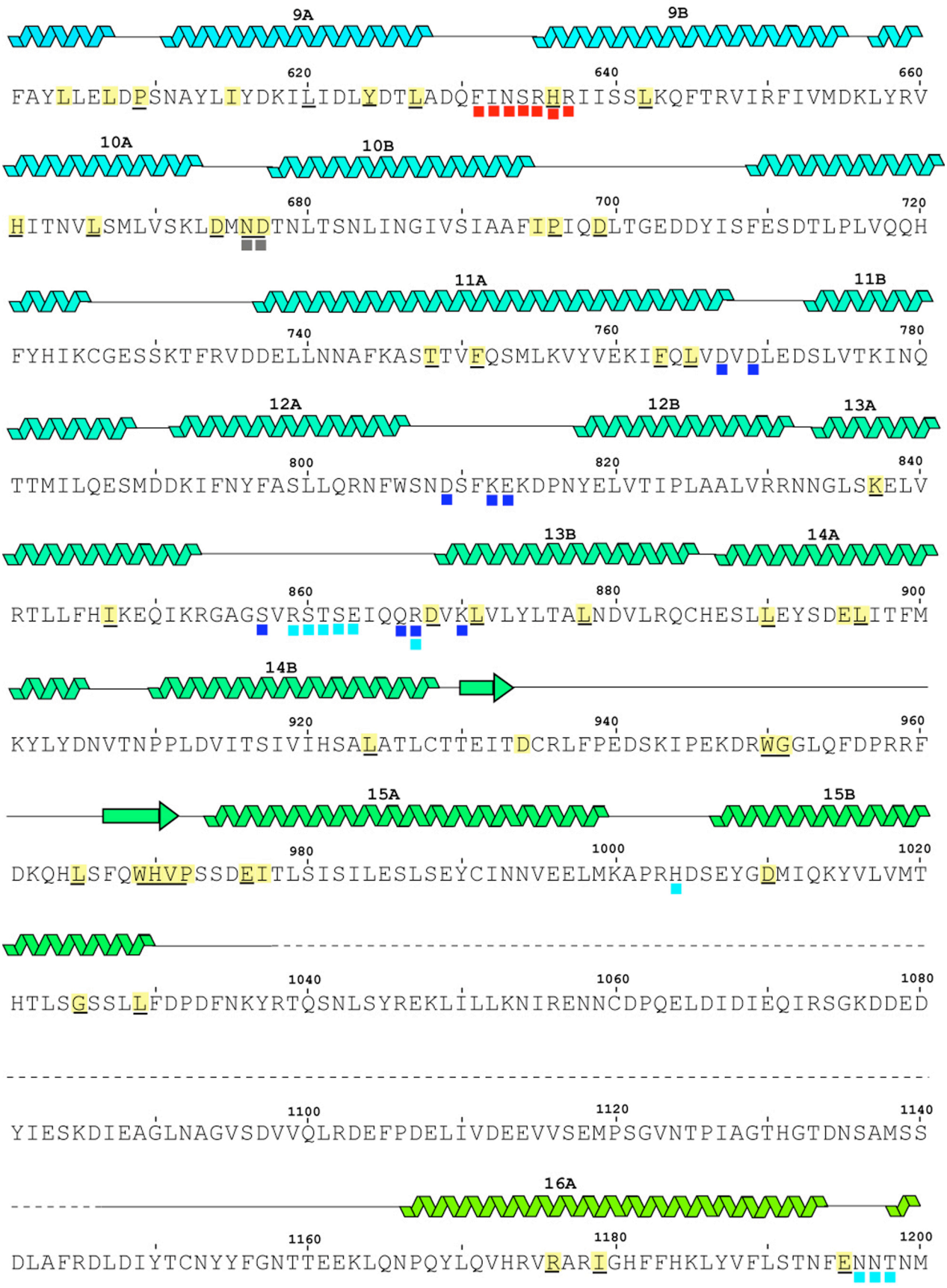
9A
9B
620
640
660
FAYLLELDPSNAYLIYDKILIDLYDTLADQFINSRHRIISSLKQFTRVIRFIVMDKLYRV
10A
10B
680
700
720
HITNVLSMLVSKLDMNDTNLTSNLINGIVSIAAFIPIQDLTGEDDYISFESDTLPLVQQH
11A
11B
740
760
780
FYHIKCGESSKTFRVDDELLNNAFKASTTVFQSMLKVYVEKIFQLVDVDLEDSLVTKINQ
12A
12B
13A
800
820
840
TTMILQESMDDKIFNYFASLLQRNFWSNDSFKEKDPNYELVTIPLAALVRRNNGLSKELV
13B
14A
860
880
900
RTLLFHIKEQIKRGAGSVRSTSEIQQRDVKLVLYLTALNDVLRQCHESLLEYSDELITFM
14B
920
940
960
KYLYDNVTNPPLDVITSIVIHSALATLCTTEITDCRLFPEDSKIPEKDRWGGLQFDPRRF
15A
15B
980
1000
1020
DKQHLSFQWHVPSSDEITLSISILESLSEYCINNVEELMKAPRHDSEYGDMIQKYVLVMT
1040
1060
1080
HTLSGSSLLFDPDFNKYRTQSNLSYREKLILLKNIRENNCDPQELDIDIEQIRSGKDDED
1100
1120
1140
YIESKDIEAGLNAGVSDVVQLRDEFPDELIVDEEVVSEMPSGVNTPIAGTHGTDNSAMSS
16A
1160
1180
1200
DLAFRDLDIYTCNYYFGNTTEEKLQNPQYLQVHRVRARIGHFFHKLYVFLSTNFENNTNM

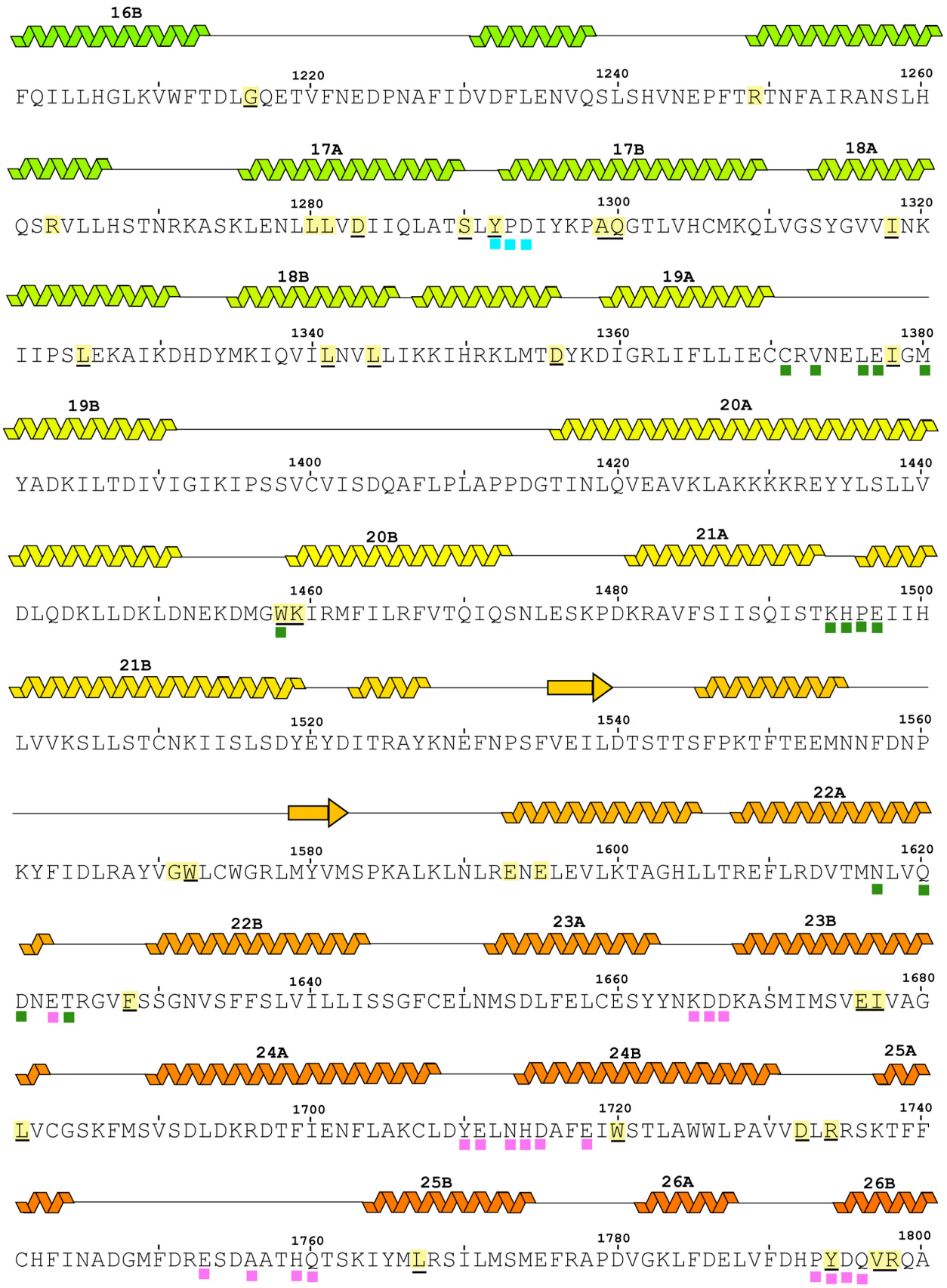
16B
1220
1240
1260
FQILLHGLKVWFTDLGQETVFNEDPNAFIDVDFLENVQSLSHVNEPFTRTNFAIRANSLH
17A
17B
18A
1280
1300
1320
QSRVLLHSTNRKASKLENLLLVDIIQLATSLYPDIYKPAQGTLVHCMKQLVGSYGVVINK
18B
19A
1340
1360
1380
IIPSLEKAIKDHDYMKIQVILNVLLIKKIHRKLMTDYKDIGRLIFLLIECCRVNELEIGM
19B
20A
1400
1420
1440
YADKILTDIVIGIKIPSSVCVISDQAFLPLAPPDGTINLQVEAVKLAKKKKREYYLSLLV
20B
21A
1460
1480
1500
DLQDKLLDKLDNEKDMGWKIRMFILRFVTQIQSNLESKPDKRAVFSIISQISTKHPEIIH
21B
1520
1540
1560
LVVKSLLSTCNKIISLSDYEYDITRAYKNEFNPSFVEILDTSTTSFPKTFTEEMNNFDNP
22A
1580
1600
1620
KYFIDLRAYVGWLCWGRLMYVMSPKALKLNLRENELEVLKTAGHLLTREFLRDVTMNLVQ
22B
23A
23B
1640
1660
1680
DNETRGVFSSGNVSFFSLVILLISSGFCELNMSDLFELCESYYNKDDKASMIMSVEIVAG
24A
24B
25A
1700
1720
1740
LVCGSKFMSVSDLDKRDTFIENFLAKCLDYELNHDAFEIWSTLAWWLPAVVDLRRSKTFF
25B
26A
26B
1760
1780
1800
CHFINADGMFDRESDAATHQTSKIYMLRSILMSMEFRAPDVGKLFDELVFDHPYDQVRQA

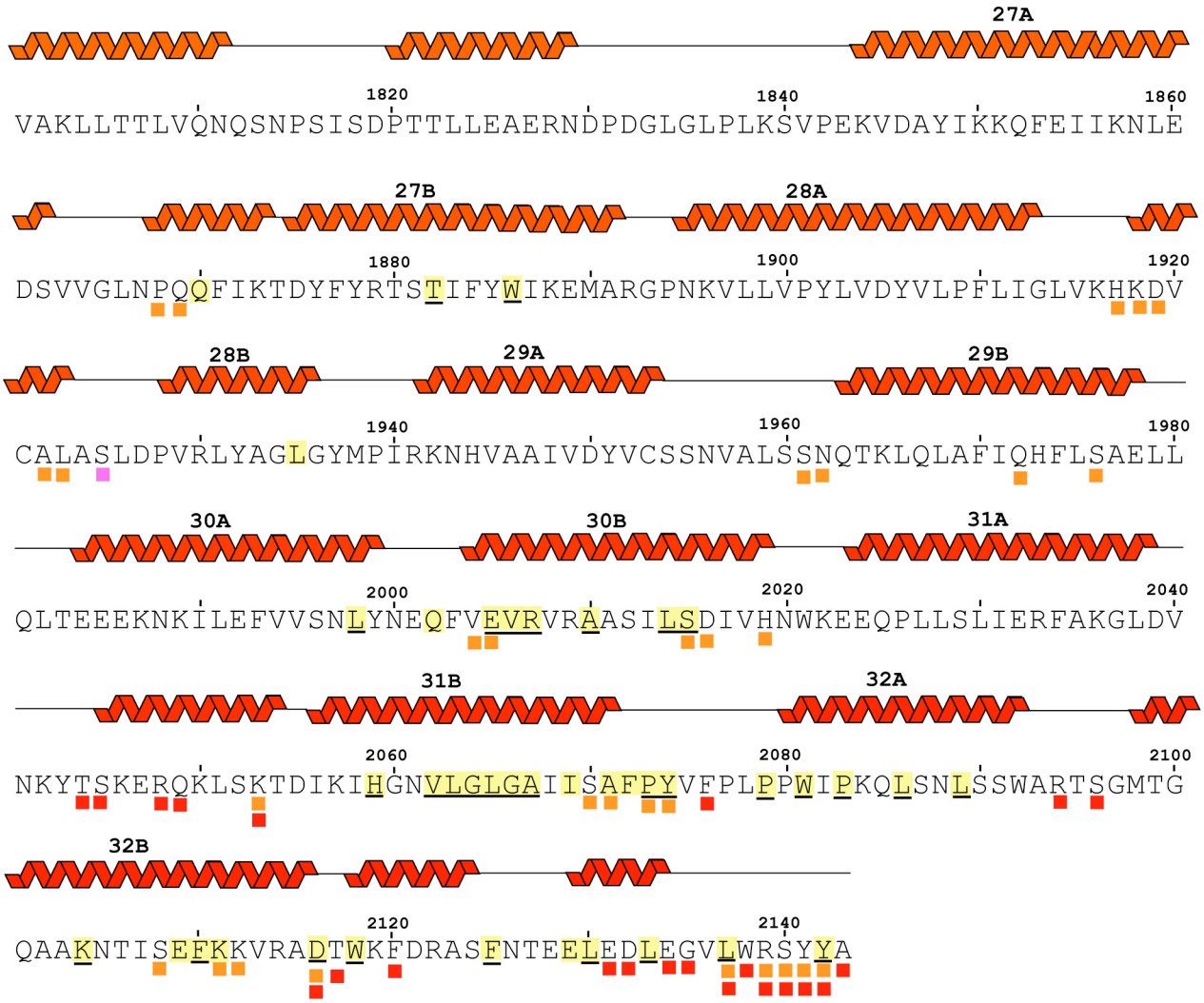
27A
1820
1840
1860
VAKLLTTLVQNQSNPSISDPTTLLEAERNDPDGLGLPLKSVPEKVDAYIKKQFEIIKNLE
27B
28A
1880
1900
1920
DSVVGLNPQQFIKTDYFYRTSTIFYWIKEMARGPNKVLLVPYLVDYVLPFLIGLVKHKDV
28B
29A
29B
1940
1960
1980
CALASLDPVRLYAGLGYMPIRKNHVAAIVDYVCSSNVALSSNQTKLQLAFIQHFLSAELL
30A
30B
31A
2000
2020
2040
QLTEEEKNKILEFVVSNLYNEQFVEVRVRAASILSDIVHNWKEEQPLLSLIERFAKGLDV
31B
32A
2060
2080
2100
NKYTSKERQKLSKTDIKIHGNVLGLGAIISAFPYVFPLPPWIPKQLSNLSSWARTSGMTG
32B
2120
2140
QAAKNTISEFKKVRADTWKFDRASFNTEELEDLEGVLWRSYYA

The 46 sequences used in the alignment to define conserved residues:

gi|37362646|ref|NP_116648.2| [Saccharomyces cerevisiae]
gi|156844582|ref|XP_001645353.1| [Vanderwaltozyma polyspora]
gi|50287269|ref|XP_446064.1| [Candida glabrata]
gi|45201074|ref|NP_986644.1| [Ashbya gossypii]
gi|50308975|ref|XP_454493.1|[Kluyveromyces lactis]
gi|50426149|ref|XP_461671.1| [Debaryomyces hansenii]
gi|150865341|ref|XP_001384517.2|[Pichia stipitis]
gi|68479947|ref|XP_716023.1| [Candida albicans]
gi|149239843|ref|XP_001525797.1|[Lodderomyces elongisporus]
gi|190348667|gb|EDK41164.2| [Pichia guilliermondii]
gi|50551363|ref|XP_503155.1|[Yarrowia lipolytica]
gi|67538874|ref|XP_663211.1|[Aspergillus nidulans]
gi|145257943|ref|XP_001401896.1| [Aspergillus niger]
gi|164425515|ref|XP_960116.2|[Neurospora crassa OR74A]
gi|171682604|ref|XP_001906245.1|[Podospora anserina]
gi|46124079|ref|XP_386593.1|[Gibberella zeae]
gi|154287488|ref|XP_001544539.1|[Ajellomyces capsulatus]
gi|154312206|ref|XP_001555431.1|[Botryotinia fuckeliana]
gi|156064295|ref|XP_001598069.1| [Sclerotinia sclerotiorum]
gi|169606348|ref|XP_001796594.1|[Phaeosphaeria nodorum]
gi|145607561|ref|XP_361868.2|[Magnaporthe grisea]
gi|119194335|ref|XP_001247771.1|[Coccidioides immitis]
gi|121707973|ref|XP_001271992.1|[Aspergillus clavatus]
gi|115391253|ref|XP_001213131.1|[Aspergillus terreus]
gi|119500344|ref|XP_001266929.1|[Neosartorya fischeri]
gi|169771439|ref|XP_001820189.1|[Aspergillus oryzae]
gi|70993706|ref|XP_751700.1|[Aspergillus fumigatus]
gi|189193275|ref|XP_001932976.1| [Pyrenophora tritici-repentis]
gi|170086077|ref|XP_001874262.1| [Laccaria bicolor S238N-H82]
gi|170084821|ref|XP_001873634.1| [Laccaria bicolor S238N-H82]
gi|195997553|ref|XP_002108645.1| [Trichoplax adhaerens]
gi|149449017|ref|XP_001517136.1| [Ornithorhynchus anatinus]
gi|126304432|ref|XP_001382168.1| [Monodelphis domestica]
gi|189524182|ref|XP_001333755.2| [Danio rerio]
gi|73970154|ref|XP_531823.2| [Canis familiaris]
gi|194220729|ref|XP_001497130.2| [Equus caballus]
gi|119903486|ref|XP_606554.3| [Bos taurus]
gi|163644283|ref|NP_055429.2| [Homo sapiens]
gi|66801317|ref|XP_629584.1| [Dictyostelium discoideum AX4]
gi|147906041|ref|NP_001084866.1| [Xenopus laevis]
gi|158290777|ref|XP_312339.4| [Anopheles gambiae str. PEST]
gi|91083491|ref|XP_972018.1| [Tribolium castaneum]
gi|149044860|gb|EDL98046.1| [Rattus norvegicus]
gi|117956381|ref|NP_598774.2| [Mus musculus]
gi|170055259|ref|XP_001863503.1| [Culex pipiens quinquefasciatus]
gi|157110835|ref|XP_001651267.1| [Aedes aegypti]

Figure S2, related to Figure 2B

This is the same as Figure 2B but also includes the closed conformation. Proteasome as seen in: Blm10 complex, white; PA26 complex (pdb 1z7q), yellow; unliganded proteasome (pdb 1ryp), cyan. Residues of the unliganded proteasome and proteasome in the Blm10 complex are labeled if they adopt conformations that are substantially different from that seen in the fully open conformation of the PA26 complex. N-terminal residues are disordered for α2, α3, and α4 in the Blm10 complex.

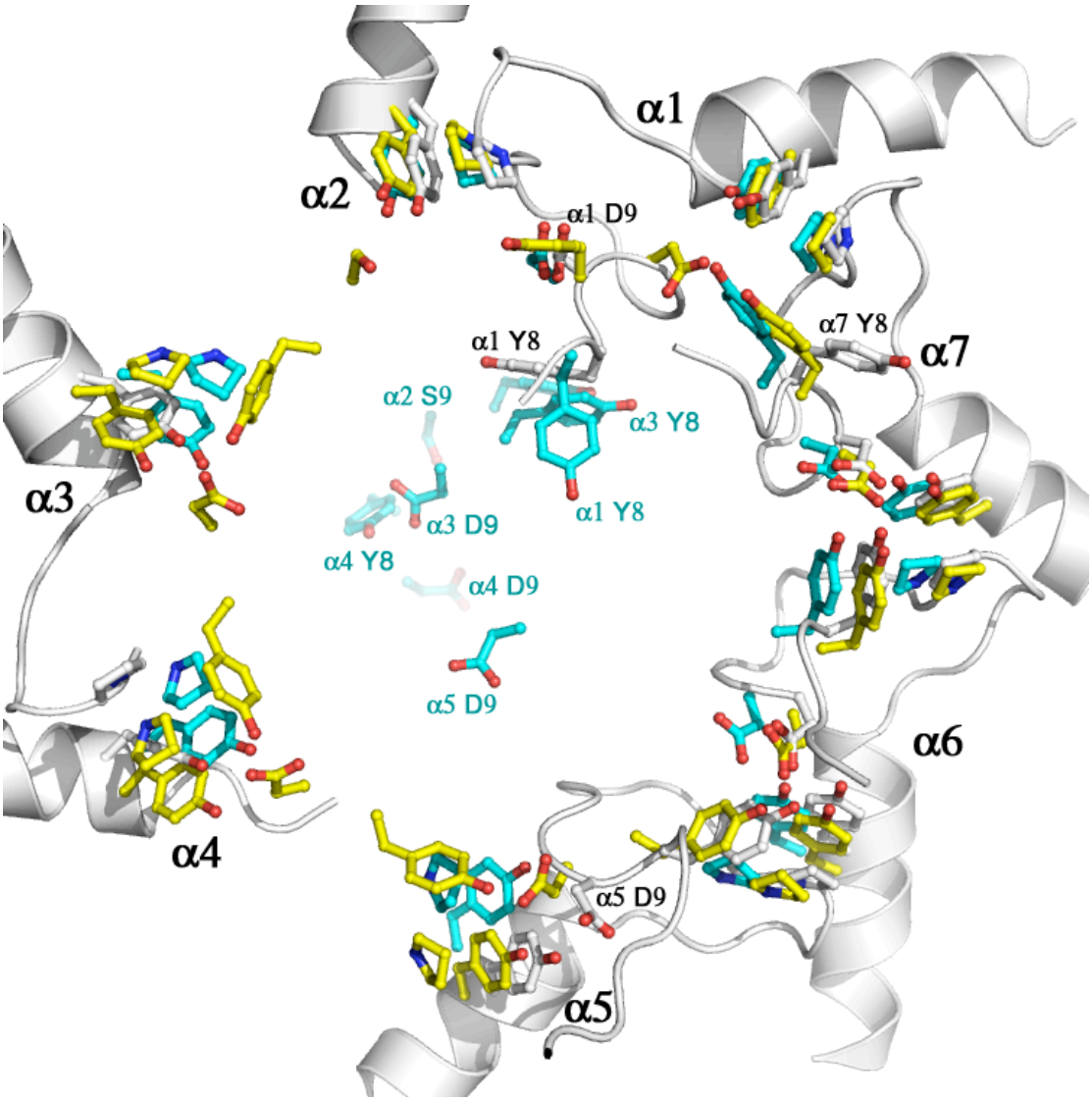

Figure S3, related to Figure 4

(A) Blm10 functions in a proteasome-dependent process

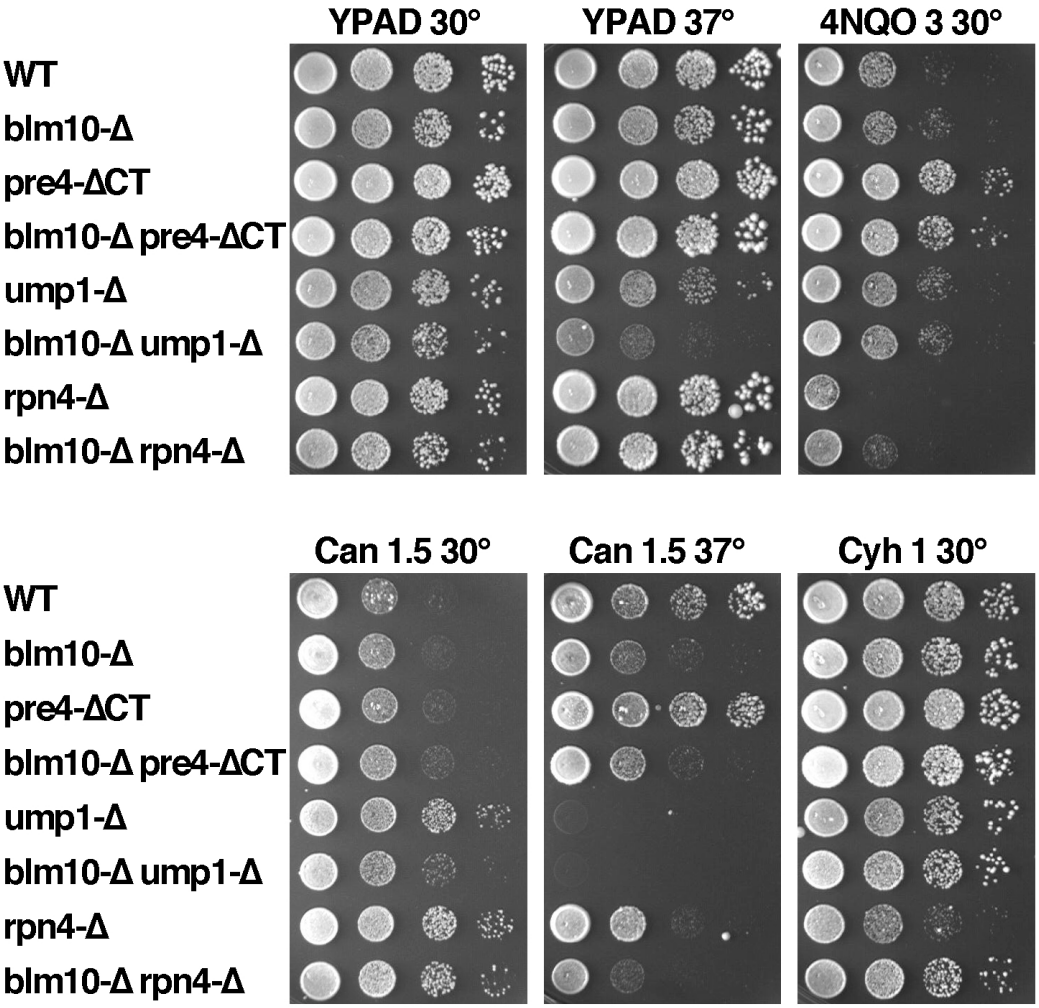

In our experiments using several strain backgrounds, loss of Blm10 did not cause significant sensitivity to any of a number of DNA damaging agents (Iwanczyk et al., 2006). Published reports indicated a role for Blm10 in the assembly or maintenance of 20S proteasomes (Fehlker et al., 2003; Marques et al., 2007), so we tested *blm10*-Δ mutants for defects associated with proteasome deficiency. Strains in the A364a background were grown to saturation in rich medium, then aliquots of 10-fold dilutions were placed on the media indicated and incubated at the temperature indicated in each panel. YPAD is rich medium, 4NQO 3 is YPAD with 3 µg/ml 4-nitroquinoline 1-oxide, Can 1.5 is synthetic medium lacking arginine and containing1.5 µg/ml canavanine, and Cyh 1 is YPAD with 1 µg/ml cycloheximide.

Elevated temperatures or inclusion of the arginine analog canavanine can stress the proteolytic system in yeast by increasing the level of unfolded or aberrantly formed proteins. For example, loss of the 20S assembly chaperone Ump1 caused slow growth at 37° (row 5, YPAD 37°). While neither elevated temperature nor canavanine alone caused a noticeable defect in growth for a *blm10*-Δ mutant, growth on a low level of canavanine at 37° was significantly impaired (compare *blm10*-Δ with WT on the 1.5 μg/ml canavanine plate incubated at 37°). Further, combining both *blm10*-Δ and *ump1*-Δ deletions caused an enhanced growth defect relative to the *ump1*-Δ strain on YPAD at 37°. These observations demonstrate that cells lacking Blm10 have impaired ability to respond to proteolytic stress, possibly due to inadequate proteasome assembly.

It was recently reported that combining *blm10*-Δ with a deletion of the C-terminal 19 residues of the 20S subunit Pre4 (β7) caused strong temperature sensitivity (Marques et al., 2007). We have been unable to reproduce this result using strains in the A364a background, as single and double mutants each grew at equivalent rates at 37° (rows 3 and 4 in the figure) or at 38° (not shown), the maximal permissive temperature for this strain background. To determine whether this difference is due to the different strain backgrounds used, we obtained the strains used by Marques et al. (2007) in the JD47-13c background. After switching the mating type of one strain we performed a genetic cross to generate double *blm10*-Δ *pre4*-Δ*CT* mutants by segregation, instead of the procedure described previously that involved sequential integration of mutations (Marques et al., 2007). Once again, none of the double mutants isolated from the cross displayed temperature sensitivity. Because the *pre4*-Δ*CT* allele used by Marques et al. was not marked, we scored it using a PCR test and verified a subset of the results by DNA sequencing. To further confirm this result, we introduced a similar *pre4*-Δ*CT* mutation into JD47-13c but this time with the *URA3* gene inserted adjacent to the deletion. This allowed a much larger number of double mutant *blm10*-Δ *pre4*-Δ*CT* segregants to be identified and tested, but all of these also proved to be temperature resistant. We were therefore unable to observe a synthetic growth defect or temperature sensitivity for *blm10*-Δ *pre4*-Δ*CT* combinations in either of two genetic strain backgrounds. The pre4-ΔCT strains we constructed in the A364a background do display resistance to 4-nitroquinoline 1-oxide, a phenotype associated with several proteasome assembly defects (Le Tallec et al., 2007), consistent with suboptimal proteasome formation. However, this phenotype is also unaffected by loss of Blm10 (compare rows 3 and 4).

While the results above are consistent with a role for Blm10 in promoting proteasome function, note that genetic analysis of proteasomal assembly and function pathways can be difficult to interpret. For example, Ump1 is needed for normal growth during the proteolytic stress associated with elevated temperature as revealed by weak growth at 37°, but an *ump1*-Δ mutant was more resistant than a WT strain to a different proteolytic stress, the presence of a low level of canavanine (compare rows 1 and 5 in the canavanine 1.5 at 30° panel). Rpn4 is a transcription factor that upregulates proteasome gene expression under conditions of proteolytic stress (Mannhaupt et al., 1999; Xie and Varshavsky, 2001), but an *rpn4*-Δ mutant grows normally at 37°, is sensitive to 4NQO, and in our tests is more resistant than WT to canavanine at 30° but more sensitive than WT to canavanine at 37°. Unlike the *pre4*-Δ*CT* or *ump1*-Δ strains, the *rpn4*-Δ mutant is sensitive to the protein synthesis inhibitor cycloheximide (Cyh). Loss of Blm10 suppressed this defect and the 4NQO sensitivity, but enhanced the defect in growth observed for the *rpn4*-Δ strain on canavanine at 37°. Schmidt et al. (2005) found that *rpn4*-Δ caused slight sensitivity to canavanine and that *rpn4*-Δ *blm10*-Δ double mutants had a slight synthetic growth defect both on rich medium and on canavanine. These results differ from ours, possibly due to strain background differences. Alternatively, as we have found that *blm10*-Δ mutants lose mitochondrial function at a high frequency, perhaps some of the variation among different experiments can be accounted for by clonal variation. That is, different cultures will have different retention of mitochondrial function due to the stochastic nature of the loss, contributing to phenotypic variation among cultures in a given assay even when comparing different clones of the same strain.

Together these results are consistent with a role for Blm10 in a proteasome-dependent process, but they illustrate the difficulty of interpreting genetic effects when examining a factor like the proteasome that directly or indirectly alters many facets of a broad range of physiologically important processes.

(B). Loss of *BLM10* has minor effects on ROS formation and mitochondrial genome mutation

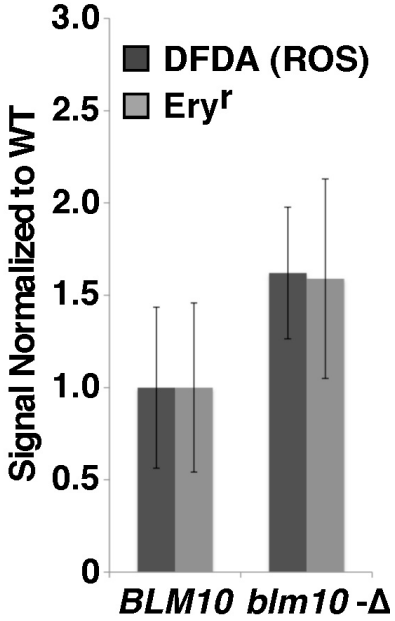

Isogenic strains with or without *BLM10* (8127-7-4, 8634-9-1) were grown to log phase in rich medium and then tested for production of reactive oxygen species (ROS) or mutation of the mitochondrial genome as detected by production of erythromycin resistant clones, essentially as described (Malc et al., 2009). Briefly, for the ROS assay, cells were collected by centrifugation, washed, then multiple aliquots were suspended in a solution containing 10 μM 2', 7'-Dichlorofluorescein diacetate (Sigma, DFDA). After incubating 30 minutes at 30° the cells were washed again, suspended in detergent and lysed by agitation with glass beads. The fluorescence of the supernatant was then tested at 520 nm with excitation at 485 nm. Signal in this assay depends on the intracellular level of ROS (Doudican et al., 2005). Dilutions of the same cultures were plated on rich medium with glycerol as the sole carbon source and containing 4 mg/ml of erythromycin. The yield of erythromycin resistant clones was then determined as an indication of the frequency of mutation of the mitochondrial rDNA locus, which determines sensitivity to this antibiotic. Three independent cultures were tested in each assay, normalized to the value obtained for the WT samples, and the average and standard deviation presented here. The average values for the WT were 1.4 fluorescence units/A660 value, and 24 erythromycin resistant colonies per 10^7 viable cells on glycerol medium lacking the drug. Loss of *BLM10* in this and other assays consistently caused slightly higher levels of ROS production and mitochondrial genome mutation, but the effect is small and not statistically significant in any single assay.

(C) Western blot showing the stability of Blm10-CTΔ3

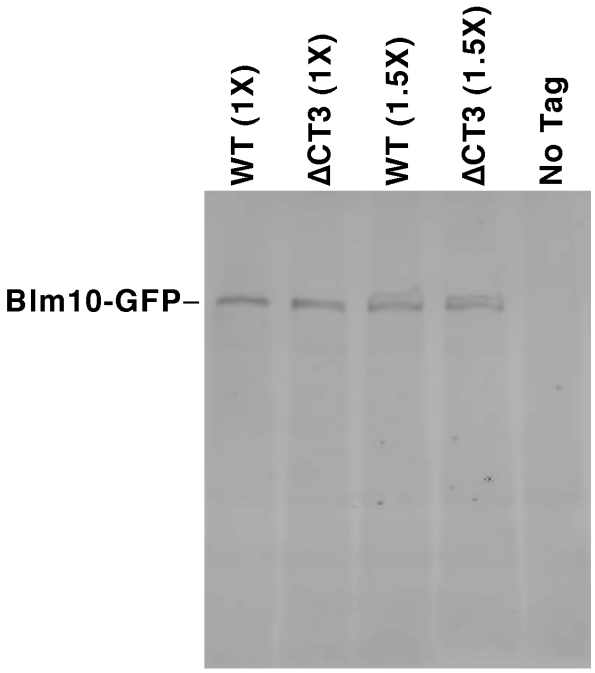

Strains 8670-1134 (WT Blm10 with GFP inserted after residue 1134), 8675-1134 (the same but with the last three residues of the Blm10 ORF deleted), and a related strain without a GFP tag were grown to log phase, treated with trichloroacetic acid, and processed for SDS-PAGE and western blotting as described (VanDemark et al., 2008). GFP was detected with a monoclonal antibody against this protein. The band indicated is the full-length fusion protein. This shows that neither deletion of the last three residues of Blm10 nor insertion of the *URA3* gene downstream of the Blm10 ORF cause detectable changes in the level of Blm10 protein. (Hua Xin, personal communication).

Table S1. Strains used, related to Figure 4

Strains were constructed using standard methods. JD47-13c and AM36 were obtained from J. Dohman (Marques et al., 2007). The final 3 residues of Blm10 were deleted by transforming with a PCR product generated using pRS406 (Brachmann et al., 1998; Longtine et al., 1998) as the template and an oligonucleotide that replaces the first tyrosine in the C-terminal ...YYA sequence with a stop codon followed by the normal 30 bp of genomic sequence found downstream of the *BLM10* gene. This inserts the URA3 gene 30 bp downstream of a C-terminally deleted allele in an otherwise normal genomic context, as confirmed by sequencing. Similar strategies were used to mark WT *BLM10* in the same position, to delete the final residue of the ORF, and to mutate the final YYA sequence to AAA.

Strain	Used in	Mating type	Genotype
A364a genetic background:			
2268-1-1	Fig 5	*MATa*	*ura3-Δ0 leu2-Δ0 trp1-Δ2 his7 blm10-Δ(::LEU2)*
7860-6-4	Fig 5	*MATa*	*ura3-Δ0 leu2-Δ0 trp1-Δ2 his7*
8015-4-1	Fig 5	*MATa*	*ura3-Δ0 leu2-Δ0 trp1-Δ2 his7 blm10-Δ(::TRP1)*
8127-5-1	Fig 5	*MATa*	*ura3-Δ0 leu2-Δ0 trp1-Δ2 his7 lys2-128∂*
8127-5-2	Fig S2	*MATa*	*ura3-Δ0 leu2-Δ0 trp1-Δ2 his3 lys2-128∂*
8127-7-4	Fig 5, S4	*MATa*	*ura3-Δ0 leu2-Δ0 trp1-Δ2 his3 lys2-128∂*
8130-1	Fig 5	*MATa*	*ura3-Δ0 leu2-Δ0 trp1-Δ2 his7 blm10-Δ(::KanMX)*
8151-1-1	Fig 5	*MATa*	*ura3-Δ0 leu2-Δ0 trp1-Δ2 his7 lys2-128∂*
8386-7-2	Fig 5	*MATa*	*ura3-Δ0 leu2-Δ0 trp1-Δ2 his7 lys2-128∂*
8571-2-1	Fig S2	*MATa*	*ura3-Δ0 leu2-Δ0 trp1-Δ2 his3 lys2-128∂ pre4-CTΔ19(URA3)*
8574-1-3	Fig S2	*MATa*	*ura3-Δ0 leu2-Δ0 trp1-Δ2 his3 lys2-128∂ rpn4-Δ(::KanMX)*
8577-6-1	Fig 5	*MATa*	*ura3-Δ0 leu2-Δ0 trp1-Δ2 his7 lys2-128∂ blm10-Δ(::LEU2)*
8578-2-4	Fig S2	*MATa*	*ura3-Δ0 leu2-Δ0 trp1-Δ2 his3 lys2-128∂ blm10-Δ(::LEU2) rpn4-Δ(::KanMX*
8578-7-1	Fig S2	*MATa*	*ura3-Δ0 leu2-Δ0 trp1-Δ2 his3 lys2-128∂ blm10-Δ(::LEU2)*
8579-6-3	Fig 5	*MATa*	*ura3-Δ0 leu2-Δ0 trp1-Δ2 his7 lys2-128∂ blm10-Δ(::LEU2)*
8583-2-1	Fig S2	*MATa*	*ura3-Δ0 leu2-Δ0 trp1-Δ2 his3 lys2-128∂ blm10-Δ(::LEU2) pre4-CTΔ19(UR*
8628-1-1	Fig 5	*MATa*	*ura3 leu2 trp1 his3 lys2-128∂ blm10-CTΔ3(URA3)*
8634-9-1	Fig 5, S4	*MATa*	*ura3-Δ0 leu2-Δ0 trp1-Δ2 his3 lys2-128∂ blm10-Δ(::LEU2)*
8647-9-2	Fig 5	*MATa*	*ura3 leu2 trp1 his7 lys2-128∂ blm10-Δ(::KanMX)*
8664-1-3	Fig 5	*MATa*	*ura3 leu2 trp1 his7 lys2-128∂ blm10-CTΔ3(URA3)*
8685	Fig 5	*MATa*	*ura3-Δ0 leu2-Δ0 trp1-Δ2 his7 lys2-128∂ blm10-YYA2141-2143AAA(URA3)*
8670-1134	Fig S5	*MATa*	*ura3-Δ0 leu2-Δ0 trp1-Δ2 his7 lys2-128∂ BLM10(1134-GFP)*
8675-1134	Fig S5	*MATa*	*ura3-Δ0 leu2-Δ0 trp1-Δ2 his7 lys2-128∂ blm10-ΔCT3(1134-GFP, URA3)*
8688	Fig 5	*MATa*	*ura3-Δ0 leu2-Δ0 trp1-Δ2 his7 lys2-128∂ blm10-*2144A(URA3)*
8689	Fig 5	*MATa*	*ura3-Δ0 leu2-Δ0 trp1-Δ2 his7 lys2-128∂ blm10-CTΔ1(URA3)*
8690	Fig 5	*MATa*	*ura3-Δ0 leu2-Δ0 trp1-Δ2 his7 lys2-128∂ BLM10(URA3)*
S288c genetic background			
8266-7-5a	Fig 5	*MATa*	*leu2-Δ1 trp1-Δ63 ura3-52 his4-912∂ lys2-128∂*
8358-T1	Fig 5	*MATa*	*leu2-Δ1 trp1-Δ63 ura3-52 his4-912∂ lys2-128∂ blm10-Δ(::TRP1)*
W303 genetic background			
8025-2-3	Fig 5	*MATa*	*ade2 can1 his3 ura3 leu2 trp1 adh4:URA3*
8132	Fig 5	*MATa*	*ade2 can1 his3 ura3 leu2 trp1 adh4:URA3 blm10-Δ(::TRP1)*
JD47-13c genetic background			
JD47-13c	Fig 5	*MATa*	*his3-Δ200 leu2-3,112 lys2-801 trp1-Δ63 ura3-52*
AM36	Fig 5	*MATa*	*his3-Δ200 leu2-3,112 lys2-801 trp1-Δ63 ura3-52 blm10-Δ(::KanMX4)*

Supplementary Experimental Procedures

Protein Preparation

Double capped *S. cerevisiae* proteasome:Blm10 and proteasome:Δ50Blm10 complexes were prepared largely as described (Iwanczyk et al., 2006). Briefly, *S. cerevisiae* strain SDL135 expressing proteasome subunit Pre1/β4 tagged with protein A at the C-terminus (Leggett et al., 2002) (kind gift of Daniel Finley and David Leggett) was grown in a 36 L fermentor in YPD+glucose at 30°C for 2 days to saturation, and harvested by centrifugation. Polyhistidine-tagged Blm10 was expressed from pTF155/pCPH1327 (full length) or pCPH1328 (Δ50) in a 36L fermentor or shaker flasks in synthetic medium with raffinose to an OD^{600} of 0.7 at 30°C, whereupon expression was induced by the addition of galactose to 1.1% and the culture grown overnight and harvested by centrifugation. Cell lysis was performed under liquid nitrogen using a freezer mill 6850 pulverizor (SPEX CentriPrep Group). Subsequent steps were performed at 4°C. Typical preparations started with 80g of cell paste expressing tagged proteasome and 80g of cell paste expressing Blm10, and followed the published protocol (Iwanczyk et al., 2006) to give a typical yield of 2-4 mg of complex. Protein was concentrated to 20-25 mg/ml in 50mM Tris pH 7.5, 50mM NaCl, 1mM EDTA, and 0.5mM dithiothreitol (DTT) using a spin filtration device. The concentrated protein was buffer exchanged in the same solution with fresh DTT using a G50-sephadex spin column.

Crystallization

Immediately prior to setting up crystallization trials, the protein sample was centrifuged at 16,000 *g* at 4°C for 10 minutes. Blm10:proteasome complex crystals were grown by vapor diffusion in drops comprising 0.5μL protein and 0.5μL reservoir against a reservoir of 5-6% PEG 8k, 0.1M Na/K phosphate pH 6.2, 0.2M NaCl, and 18-30% of ethylene glycol. Crystals were harvested by addition of ~50 μL of well solution to the drop immediately prior to suspending the crystal in a nylon loop and plunging into liquid nitrogen. Crystals with full-length Blm10 and Blm10 missing the first 50 amino acid residues (Blm10Δ50) grew under the same conditions and generally had similar morphologies, although the Blm10Δ50 complex crystals grew more reproducibly in about 2-3 weeks and diffracted more strongly. Growth of full-length Blm10 complex crystals took from weeks to months and was highly non-reproducible, with the large majority of preparations not yielding usable crystals. Both of the constructs had N-terminal extensions of 12 histidine residues, and started with the sequence H_{12}-G-

T^2 or H_{12}-GT-D^{51}. The polyhistidine tags were not removed prior to setting up crystallization trials. The full-length Blm10:proteasome crystals were poorly isomorphous and showed large variation in cell dimensions and even in space group.

Structure Determination

Diffraction data were collected at the National Synchrotron Light Source beamline X29 and processed using HKL (Otwinowski and Minor, 1997). Data were collected from the various crystals (Table 1) at 100K and at the wavelength indicated: c158 1.1 Å; c164 1.0 Å; c172 1.0688 Å; c280 1.0809 Å; c290 1.0 Å; c292 1.0642 Å. Many of the crystallographic calculations were performed using programs of the CCP4 suite (Collaborative Computational Project, 1994). The various crystal forms were phased by molecular replacement with PHASER (McCoy et al., 2007) using the unliganded structure of the *S. cerevisiae* proteasome (Groll et al., 1997) (pdb code 1ryp) as the search model. Map quality was greatly improved by non-crystallographic symmetry (NCS) averaging over the multiple copies of half proteasome:Blm10 complexes in the asymmetric unit and averaging between different crystal forms using DMMULTI (Cowtan, 1994). Map quality was further improved by application of a -50 $Å^2$ sharpening factor. Crystals belonging to space group $P2_1$ had four-fold NCS, and crystals belonging to space group $P2_12_12_1$ had two-fold NCS.

Model building with O (Jones et al., 1991) was aided by the identification of 20 methionine and 14 cysteine sites from crystals soaked in thimerosal, methyl mercury nitrate, or potassium platinum tetrachloride. Heavy atom derivates were prepared by adding aqueous stock solutions to the crystallization well solution to make the concentration indicated, followed by addition of 40 μL of this solution directly to the crystallization drop for the time indicated prior to mounting and plunging into liquid nitrogen: c164/FL-Thim, thimerosal, 6mM, 2 hours; c172/FL- $PtCl_4$, 6 mM, 2 hours; c290/Δ50-MeHg, $MeHgNO_2$, 1 mM, 10 minutes; c292/Δ50-$PtCl_4$, K2PtCl4 2mM, 24 hours. Due to non-isomorphism, the heavy atom derivative structures were determined individually by molecular replacement and their phases refined by NCS averaging. Anomalous difference Fourier maps were found to be more sensitive than isomorphous difference maps for the location of heavy atoms.

The best diffracting crystal structure was refined with REFMAC5 (Murshudov et al., 1997) and rebuilt with KiNG (Davis et al., 2007), with the final refinement calculations performed using Phenix (Adams

et al., 2002). All measured reflections (except the test set) were used in refinement, regardless of I/σ(I) value, up to a Bragg spacing of 3.0 Å, at which point the σ_A value falls precipitously (DeLaBarre and Brunger, 2006). No solvent molecules were included in the model. NCS restraints were set automatically in Phenix and only minor deviations from NCS are apparent. Stereochemistry was assessed using MolProbity (Davis et al., 2007), and the overall clashscore was 70% for the Blm10 portion of the structure in comparison with other structures reported at 3.4 Å resolution. The clashscore was 89% for the proteasome portion of the structure. Molprobity evaluated 87.8% of residues as possessing favored Ramachandran angles and 2.8% as being outliers. The following residues lacked defined density and have been omitted from the model. Blm10: N-terminus to Ser78, Asp155-Ala238, Arg1038-Asp1146. Proteasome: α1 before Ala10, α2 before Gln20, α3 before Ser14, α4 before Ile17, α7 before Gly4. All other proteasome residues that were present in the search model were also included in the Blm10 complex refinement. Crystallographic statistics are given in Table 1. The figures were made with PyMol (DeLano, 2002).

Supplementary References

Adams, P.D., Grosse-Kunstleve, R.W., Hung, L.W., Ioerger, T.R., McCoy, A.J., Moriarty, N.W., Read, R.J., Sacchettini, J.C., Sauter, N.K., and Terwilliger, T.C. (2002). PHENIX: building new software for automated crystallographic structure determination. Acta Crystallogr D Biol Crystallogr *58*, 1948-1954.

Brachmann, C.B., Davies, A., Cost, G.J., Caputo, E., Li, J., Hieter, P., and Boeke, J.D. (1998). Designer deletion strains derived from Saccharomyces cerevisiae S288C: a useful set of strains and plasmids for PCR-mediated gene disruption and other applications. Yeast *14*, 115-132.

Collaborative Computational Project, N. (1994). The CCP4 suite: programs for protein crystallography. Acta Crystallogr D Biol Crystallogr *50*, 760-763.

Cowtan, K.D. (1994). 'dm': An automated procedure for phase improvement by density modification. Joint CCP4 and ESF-EACBM newsletter on protein crystallography *31*, 34-38.

Davis, I.W., Leaver-Fay, A., Chen, V.B., Block, J.N., Kapral, G.J., Wang, X., Murray, L.W., Arendall, W.B., 3rd, Snoeyink, J., Richardson, J.S.*, et al.* (2007). MolProbity: all-atom contacts and structure validation for proteins and nucleic acids. Nucleic Acids Res *35*, W375-383.

DeLaBarre, B., and Brunger, A.T. (2006). Considerations for the refinement of low-resolution crystal structures. Acta Crystallogr D Biol Crystallogr *62*, 923-932.

DeLano, W.L. (2002). The PyMOL Molecular Graphics System (DeLano Scientific, San Carlos, CA, USA.).

Doudican, N.A., Song, B., Shadel, G.S., and Doetsch, P.W. (2005). Oxidative DNA damage causes mitochondrial genomic instability in Saccharomyces cerevisiae. Mol Cell Biol *25*, 5196-5204.

Gouet, P., Courcelle, E., Stuart, D.I., and Metoz, F. (1999). ESPript: analysis of multiple sequence alignments in PostScript. Bioinformatics *15*, 305-308.

Jones, T.A., Zou, J.Y., Cowan, S.W., and Kjeldgaard, M. (1991). Improved methods for building protein models in electron density maps and the location of errors in these models. Acta Crystallogr A *47 (Pt 2)*, 110-119.

Le Tallec, B., Barrault, M.B., Courbeyrette, R., Guerois, R., Marsolier-Kergoat, M.C., and Peyroche, A. (2007). 20S proteasome assembly is orchestrated by two distinct pairs of chaperones in yeast and in mammals. Mol Cell *27*, 660-674.

Leggett, D.S., Hanna, J., Borodovsky, A., Crosas, B., Schmidt, M., Baker, R.T., Walz, T., Ploegh, H., and Finley, D. (2002). Multiple associated proteins regulate proteasome structure and function. Mol Cell *10*, 495-507.

Longtine, M.S., McKenzie, A., 3rd, Demarini, D.J., Shah, N.G., Wach, A., Brachat, A., Philippsen, P., and Pringle, J.R. (1998). Additional modules for versatile and economical PCR-based gene deletion and modification in Saccharomyces cerevisiae. Yeast *14*, 953-961.

Mannhaupt, G., Schnall, R., Karpov, V., Vetter, I., and Feldmann, H. (1999). Rpn4p acts as a transcription factor by binding to PACE, a nonamer box found upstream of 26S proteasomal and other genes in yeast. FEBS Lett *450*, 27-34.

McCoy, A.J., Grosse-Kunstleve, R.W., Adams, P.D., Winn, M.D., Storoni, L.C., and Read, R.J. (2007). Phaser crystallographic software. J Appl Cryst *40*, 658-674.

Murshudov, G.N., Vagin, A.A., and Dodson, E.J. (1997). Refinement of macromolecular structures by the maximum-likelihood method. Acta Crystallogr D Biol Crystallogr *53*, 240-255.

Ortega, J., Heymann, J.B., Kajava, A.V., Ustrell, V., Rechsteiner, M., and Steven, A.C. (2005). The axial channel of the 20S proteasome opens upon binding of the PA200 activator. J Mol Biol *346*, 1221-1227.

Otwinowski, Z., and Minor, W. (1997). Processing of X-ray diffraction data collected in oscillation mode. Methods Enzymol *276*, 307-326.

VanDemark, A.P., Xin, H., McCullough, L., Rawlins, R., Bentley, S., Heroux, A., Stillman, D.J., Hill, C.P., and Formosa, T. (2008). Structural and functional analysis of the Spt16p N-terminal domain reveals overlapping roles of yFACT subunits. J Biol Chem *283*, 5058-5068.

Xie, Y., and Varshavsky, A. (2001). RPN4 is a ligand, substrate, and transcriptional regulator of the 26S proteasome: a negative feedback circuit. Proc Natl Acad Sci U S A *98*, 3056-3061.